



HAL
open science

Microtubule-associated protein 9 (Map9/Asap) is required for the early steps of zebrafish development

Laura Fontenille, Sylvie Rouquier, Georges Lutfalla, Dominique Giorgi

► To cite this version:

Laura Fontenille, Sylvie Rouquier, Georges Lutfalla, Dominique Giorgi. Microtubule-associated protein 9 (Map9/Asap) is required for the early steps of zebrafish development. *Cell Cycle*, 2014, 13 (7), pp.1101-1114. 10.4161/cc.27944 . hal-02088317

HAL Id: hal-02088317

<https://hal.umontpellier.fr/hal-02088317>

Submitted on 11 Apr 2019

HAL is a multi-disciplinary open access archive for the deposit and dissemination of scientific research documents, whether they are published or not. The documents may come from teaching and research institutions in France or abroad, or from public or private research centers.

L'archive ouverte pluridisciplinaire **HAL**, est destinée au dépôt et à la diffusion de documents scientifiques de niveau recherche, publiés ou non, émanant des établissements d'enseignement et de recherche français ou étrangers, des laboratoires publics ou privés.

Microtubule-associated protein 9 (Map9/Asap) is required for the early steps of zebrafish development

Laura Fontenille^{1,2,§}, Sylvie Rouquier¹, Georges Lutfalla³, Dominique Giorgi^{1,*}

¹Institute of Human Genetics, UPR 1142, CNRS, 141 rue de la Cardonille, 34396 Montpellier, France,

²Université de Montpellier 1, France

³Dynamique des Interactions Membranaires Normales et Pathologiques, UMR 5235, CNRS, Universités de Montpellier 1&2, France.

[§]Current affiliation: DIMNP, UMR 5235, CNRS, Universités de Montpellier 1&2, France

Running Title: Map9 is required for zebrafish development

*To whom correspondence should be addressed. Tel: 33-499619993 Fax: 33-499619935; E-mail: giorgi@igh.cnrs.fr.

Keywords: microtubule-associated protein, microtubules, zebrafish, knockdown, mitosis, yolk syncytial layer, epiboly, gastrulation, development

Abbreviations: ASAP, aster-associated protein; *aurka*, aurora kinase a; *bon*, bonnie and clyde; *cyc*, cyclops; *dnah9*, dynein, axonemal, heavy polypeptide 9; *eomesa*, *b*, eomesodermins a, b; *foxa2*, forkhead box A2; *gata5*, gata-binding protein 5; GFP, green fluorescent protein; *gsc*, goosecoid; hpf, hours post-fecundation; *igu*, iguana; KV, K pffer's vesicle; LR, left-right; MAP, microtubule-associated protein; ISH, *in situ* hybridization; LPM, lateral plate mesoderm; MO, morpholino oligonucleotide; MT, microtubule; *nipbla*, *b*, nipped-b-like homologs a, b; *ntla*, no tail a; *oep*; one-eyed pinhead; ORF, open reading frame; PBS, phosphate-buffered saline; *plk1*, 4, polo-like kinases 1, 4; *shha*, sonic hedgehog a; *smo*, smoothened; *sox32* and *sox17*, SRY-box containing genes 32 and 17;

spaw, southpaw; *sqt*, squint; TGF β ; *tp53*, tumor protein 53; TUNEL, terminal deoxynucleotidyl transferase-mediated fluorescein-dUTP nick-end labeling assay; YFP, yellow fluorescent protein; YSL, yolk syncytial layer

Abstract

Microtubules are structural components of the cell cytoskeleton and key factors for mitosis and ciliogenesis in eukaryotes. The regulation of MT dynamics requires non-motor MAPs. We previously showed that, in human cells in culture, MAP9 (also named ASAP) is involved in MT dynamics and is essential for mitotic spindle formation and mitosis progression. Indeed, misexpression of MAP9 leads to severe mitotic defects and cell death. Here, we investigated the *in vivo* role of *map9* during zebrafish development. *Map9* is expressed mainly as a maternal gene. Within cells, Map9 is associated with the MT network of the mitotic spindle and with centrosomes. Morpholino-mediated depletion of *map9* leads to early development arrest before completion of epiboly. Map9 localizes to the MT array of the YSL. This MT network is destroyed in Map9-depleted embryos and injection of anti-*map9* morpholinos directly in the nascent YSL leads to arrest of epiboly/gastrulation. Finally, *map9* knockdown deregulates the expression of genes involved in endodermal differentiation, dorso-ventral and left-right patterning, and other MT-based functions. At low morpholino doses, the surviving embryos show dramatic developmental defects, spindle and mitotic defects and increased apoptosis. Our findings suggest that *map9* is a crucial factor in early zebrafish development by regulating different MT-based processes.

Introduction

MTs are fibrillar structures that are present in all eukaryotic cells. The centrosome is the primary MT-organizing centre of animal cells and is involved in regulating cell motility and polarity in interphase as well as in organizing the spindle poles during mitosis. The centriole is the core centrosomal component. During development and also in cultured cells, centrioles are involved in the formation of the mitotic spindle poles and the basal body of primary cilia. Cell divisions require coordination between chromosome segregation by the mitotic spindle (a bipolar MT-based structure) and cell

cleavage by the cytokinetic apparatus. Spindle assembly and chromosome segregation depend on many factors ^{1,2} that regulate MT dynamics ³⁻⁵, including also non-motor MAPs. In fish, the YSL is an extraembryonic tissue that forms at the surface of the yolk and that drives epiboly during which the blastoderm spreads over the yolk cell toward the vegetal pole ⁶⁻⁸. YSL movements rely heavily on a specific and dense MT network, and during epiboly/gastrulation YSL emits Nodal/TGF β signals that specify the endoderm and mesoderm cell fate ⁶.

We have recently characterized a novel human spindle MAP named ASAP or MAP9 ⁹. MAP9 overexpression induces aberrant spindles in mitosis and its depletion by RNA interference results in severe mitotic defects that lead to aneuploidy and/or cell death. These findings indicate that MAP9 has a crucial role in the organization of the bipolar mitotic spindle and in mitotic progression. MAP9 is phosphorylated by the mitotic kinases Aurora A ¹⁰ and PLK1 ¹¹ to regulate its role in bipolar spindle assembly and centrosome integrity. TP53 is a key factor that controls the response to DNA damage, and we have shown that in response to DNA damage, MAP9 transiently accumulates and interacts with and stabilizes TP53 ¹².

As MAP9 is thought to be involved in various aspects of MT dynamics, we decided to investigate, *in vivo*, the role of *map9* during embryogenesis using zebrafish as a model. In addition to the aforementioned works to support this hypothesis, large scale studies identified MAP9 and PLK1 as ciliopathy candidate genes ¹³⁻¹⁶, and Plk1 inhibition induces growth defects in developing zebrafish embryos ^{17,18}.

Here we report that *map9* is expressed during early zebrafish development and localizes to the MTs of the mitotic spindle and to centrosomes. Inhibition of *map9* expression using oligonucleotide morpholinos blocks zebrafish development during the early steps of embryogenesis, leading to embryo death or to dramatic developmental defects. Morphant embryos display mitotic defects and increased apoptosis. Injection of anti-*map9* morpholino oligomers is associated with reduction of the MT network of the YSL and injection of morpholino directly in the nascent YSL of early embryos blocks epiboly/gastrulation. Finally, *map9* knockdown deregulates the expression of a number of genes involved mainly in the nodal pathway.

These *in vivo* results confirm the previous *in vitro* observations about ASAP/MAP9 role in regulating MT dynamics and suggest that Map9 is a key factor during the early steps of zebrafish development.

Results

Zebrafish *map9* is expressed early during embryo development

To obtain a full-length zebrafish *map9* cDNA clone, we screened the IMAGE library using the sequence of the predicted ENSDART00000133937 transcript (Ensembl), which encodes a 678 aa protein, and the partial sequence BC124374 (GenBank) that was identified as zebrafish *map9*. The clone IMAGp998O0412053Q (IMAGE ID 5413083) was ordered and fully sequenced. This 2520 bp cDNA sequence (GenBank accession number JQ768417) includes a 2037 nucleotide-long ORF that encodes a 678 aa protein with very few amino acid changes compared to the ENSDART00000133937 sequence. We also cloned and sequenced the *map9* cDNA from the zebrafish *golden* mutant. The predicted protein sequence was identical to the one encoded by the JQ768417 clone. Protein sequence comparisons show that the zebrafish Map9 protein is ~50% similar (~27% protein identity) to the human and mouse MAP9 proteins¹⁹.

A previous microarray analysis²⁰ established that, in zebrafish embryos, the level of *map9* mRNA increases between 0 and 3 hpf (~1000-cell stage²¹), then decreases quickly until 24 hpf (pharyngula, prim-5 stage) and remains stable up to the swimming larva stage (5 days post-fertilization). We confirmed these findings by quantifying *map9* mRNA expression in unfertilized eggs (0 hpf) and in embryos up to 24 hpf by qPCR (with normalization to β -actin, Figure 1A). Specifically, maternal *map9* mRNA was high in unfertilized eggs (0 hpf). *Map9* level increased between 1 and 2 hpf (64-cell stage) and then gradually decreased and remained stable from 4 hpf (sphere period) to 24 hpf. This observation suggests that, like for many maternal gene transcripts²², high *map9* level is required in the early steps of embryogenesis that are characterized by high mitosis rate, while a basal level is then sufficient for normal cell function.

***Map9* is expressed in the nervous system and is associated with the mitotic spindle**

In situ hybridization analysis of zebrafish embryos²³ showed that *map9* is expressed in the ventral

spinal cord (from the 1-4 somite to the Prim-5 stage, *i.e.* from 10 to 24 hpf), the diencephalon, the olfactory placode and the tegmentum at the Prim-5 stage, but it was not detected before 10 hpf or after 24 hpf. We tried to study the expression pattern of *map9* on whole embryos during epiboly (before 10 hpf) and in the adult, but we also did not get a significant labelling using *in situ* hybridization. However, to get information about the distribution of *map9* during epiboly, *map9* RNA was overexpressed at the 1-cell stage and the embryos were hybridized with RNA probes at ~30% epiboly (4.6 hpf, Figure S1). Although this experiment does not reveal the localization of the endogenous protein, it suggests that *map9* is ubiquitously expressed in the blastoderm, probably at the microtubule level as shown in Figures 1B and 6.

To follow Map9 expression in individual cells, we injected *in vitro* transcribed *map9*-YFP RNA in 1-2 cell stage embryos. Individual mitoses were observed at 24 hpf by confocal microscopy (Figure 1B-C). Although Map9 localization to cytoplasmic MTs was not obvious over background, Map9 co-localized with α -tubulin in the MT network of the mitotic spindle (Figure 1B), as we previously reported in other species^{9, 10, 19}. Specifically, zebrafish Map9 co-localized with MTs along the entire length of the mitotic spindle, from the centrosome to the distal ends. Like in other species, zebrafish Map9 was also localized to centrosomes, as revealed by co-localization with γ -tubulin (Figure 1C). Although this experiment relies on an overexpression procedure that may produce overexpression phenotypes, it provides valuable information about the localization of zebrafish Map9 to the mitotic spindle as we previously observed in other species using the same protocol or antibody detection^{9, 19}. The MAP domain that spans the C-terminal part of the protein (amino-acids 451-678 in zebrafish) is well conserved in distantly related species (~38% identity and >65% similarity between fish and Human) suggesting a conserved function. Also, the MIT-like domain¹⁹ (microtubule interacting and trafficking domain) is conserved in fish (amino-acids 455-533) with most of its characteristic features. In addition, experiments using a YFP- Δ CterMap9 construct lacking the MAP domain, showed a loss of fiber-like distribution of Map9 in mitotic cells, suggesting that this domain is required for zebrafish Map9 to localize to microtubules, as we previously showed in Human⁹ (Figure S2). The nuclear localization signals (NLS) found in the Human MAP domain are not conserved in fish. However another bipartite NLS was found in the same region using the pSORTII software (amino-acids 570-

587 and 598-614).

***Map9* knockdown or overexpression leads to major developmental defects**

We previously showed ⁹ that MAP9 expression must be tightly regulated in normal cells as MAP9 depletion or overexpression leads to severe mitotic defects. To understand the role of *Map9* in zebrafish development, we knocked *map9* down using morpholino oligomers (MO) that block *map9* splicing (MOex5) or translation (MO-ATG). These two MOs were injected separately into the yolk of 1-2-cell stage embryos. Although MO-ATG blocked the expression of maternal and zygotic *map9* mRNAs, comparable effects were obtained with both MOs. We tested a range of concentrations (0.25, 0.50, 0.75 and 1 pmol per embryo) and found that most of the injected embryos died before 24 hpf (70% following injection of 0.25 pmol and 100% with 0.75-1.0 pmol MOs). Conversely, non-injected embryos or embryos injected with the control MOmis MO (same sequence than MOex5 except 5 mismatches) were relatively unaffected (death rate=7% and 18%, respectively). In the rest of the study we used only MOex5. To ascertain the specificity of MOex5, we assessed *map9* expression by RT-PCR using RNA from 5 and/or 8 hpf embryos injected with MOex5, MO-ATG or control MOmis and the *map9*-specific primers ZF1/ZF8. A lower *map9* band was detected on agarose gel in MOex5 morphants at 5 hpf, suggesting that the MO could start blocking *map9* RNA splicing much earlier, but not in MO-ATG or MOmis-injected embryos (Figure 2A). The ratio between the two bands increased up to 8 hpf and then remained stable. Partial blocking by MOs are frequent ^{24, 25} and we have previously shown that mis-expression of MAP9 led to drastic effects ⁹. Sequencing of these two fragments revealed that the upper band corresponded to wild-type *map9* (newly transcribed zygotic mRNAs and maternal mRNAs left) and the lower band to a mis-spliced form in which exons 5 and 6 were deleted (Figure 2B), leading to the loss of 292 bp in the mRNA and of 97 aa in the protein sequence. However to evaluate the efficacy of MOex5, we quantified the two *map9* mRNA species by qPCR using specific primer pairs, in 8 hpf MOex5 morphants (transcription blocked) and MO-ATG morphants (translation blocked) as a control (Figure 2B, bottom panel). In MOex5 embryos, the wt *map9* mRNA is only 19% of that in MO-ATG control embryos (similar results were obtained with MOmis embryos, not shown) and the misspliced form represents 11% of total *map9* mRNA versus

background level in MO-ATG embryos. These results indicate that MOex5 blocks >80% of *map9* transcription and/or leads to abnormal misspliced mRNAs that are degraded.

Based on these results, we decided to use 1 pmol of MOs to detect early defects (<10 hpf, Figure 2 C-F) and 0.25 pmol of MOs for analysis at 24 and 48 hpf (Figure 2 G-L). Following injection of 1 pmol MOex5, embryo development was blocked at mid-epiboly (5-6 hpf) and most embryos died around 9-10 hpf because they could not complete epiboly. Few embryos injected with 0.25 pmol MOex5 survived up to 24 hpf (27%) and 48 hpf (5%), but they showed a range of complex defects, including possible embryo axis defects, large yolk, short body size, curved tail, flat head with small brain often associated with eye absence or almost no brain, abnormal somites, pericardial oedema and other features that were reminiscent of gastrulation defects (Figure 2G-L). Moreover, in MOex5 morphants the notochord was abnormal (Figure 2J, arrow in the inset; compare with Figure 2I) and the chevron structure of somites disorganized. Similar defects were observed in embryos injected with 1 pmol or 0.25 pmol of MO-ATG (data not shown). Although these morphants do not represent the main effect of *map9* knockdown (arrest of development at mid-epiboly), they provide information about the multiple effects of *map9* misexpression.

To ascertain the specificity of MOex5 effect on zebrafish embryo development, we co-injected *map9*-YFP mRNA and MOex5. However, *map9*-YFP (200 pg) only partially rescued the MOex5 phenotypes (Figure 3). About 40% of MOex5-injected embryos showed defects at mid-epiboly and died at ~9-10 hpf and 20% were blocked at the sphere stage. Conversely, about 80% of embryos co-injected with MOex5 and *map9*-YFP RNA developed normally up to mid-epiboly, but died between 9-10 and 24 hpf (similar results were obtained by co-injecting MOex5 and *map9* RNA, not shown). The percentage of embryos blocked at the sphere stage was slightly reduced. Control *map9*-YFP embryos developed normally up to mid-epiboly and also to later stages. Injection of lower amounts of *map9*-YFP RNA (45, 90 pg) did not rescue morphant phenotype (not shown) and injection of higher amounts of *map9*-YFP RNA (400 pg) resulted in overexpression phenotypes, as shown in Figure S3 and in Saffin *et al.* ⁹, and thus affected the rescue of the MOex5 phenotypes. This experiment shows that only the initiation of epiboly could be rescued but not the embryo lethality phenotype further

confirming that the Map9 level in the cells should be tightly regulated for the development to proceed correctly.

As overexpression of MAP9 in cultured human cells leads to severe mitotic defects and cell death⁹, we overexpressed Map9 also in zebrafish embryos by injecting *in vitro* transcribed *map9*-YFP mRNA in 1-cell embryos. Abnormal phenotypes (Figure S3) were observed following injection of 400 pg *map9*-YFP mRNA with a death rate of ~10% at 24hpf (Figure S3C), and similar results were obtained by injecting *map9* mRNA (not shown). About 40% of embryos displayed complex malformations, such as brain and tail underdevelopment, abnormal yolk, and in some cases severe phenotypes (Figure S3B) caused by abnormal gastrulation, similarly to what observed in MOex5 morphants.

Map9 inhibition induces apoptosis/cell death

As depletion of human MAP9 in cultured cells is associated with high cell death rate⁹, we quantified apoptosis in zebrafish embryos at 8 hpf (75% epiboly) and 24 hpf (Prim-5 stage) by TUNEL assay (Figure 4A-D). Due to the high death rate of morphants, 1-cell embryos were injected with 1 pmol MOex5 and observed at 8 hpf, or with 0.25 pmol MOex5 and observed at 24 hpf (Figure 4A-D). Although apoptosis is instrumental for proper embryo development²⁶, we detected a 4-fold increase in TUNEL-positive cells at 8 hpf and a ~9-fold increase at 24 hpf (Figure 4E, left panel) in *map9* morphants in comparison to non-injected controls. These results indicate that developmental defects in *map9* morphants are correlated to increased apoptosis. We also verified that inhibition of tp53 was not able to rescue apoptosis in MOex5 morphants (Figure 4E, right panel). To rule out the possibility that *map9* depletion and/or morpholino injection might induce *tp53* and therefore tp53-dependent cell death, we measured the relative *tp53* mRNA level by qPCR using RNA from 7 and 24 hpf control embryos and morphants, and found almost no variation of its expression (Figure 4F). By comparison, MO depletion of *plk1* or *aurora-a*, two mitotic kinases that phosphorylate Map9, induces tp53-dependent cell death by enhancing *tp53* expression by 7- to 10-fold^{27,28}. In addition, depletion of *tp53* by co-injection of MO-*tp53* with MOex5 did not rescue the embryo mortality observed in MOex5-injected embryos (Figure 4G).

***Map9* inhibition disrupts mitosis**

As knockdown of *MAP9* by RNA interference in human cells leads to incomplete mitosis⁹ and consequently to the death of more than 40% of cells, we asked whether the higher apoptosis rate observed in MOex5 morphants in comparison to controls could be linked to mitotic defects.

To test this hypothesis we first counted the mitotic cells in embryos fixed at 5 and 8 hpf after injection of MOex5 or MOmis (control) and immunostained with an anti-phosphohistone H3 antibody (pH3, a mitosis marker)²⁹ (Figure 5A-C). The number of pH3-positive cells was reduced by 35-40% in MOex5-injected embryos, suggesting an early mitotic blockade. Moreover, in MOex5 morphants, cells displayed mitotic infidelity (such as irregular spindle assembly, hypercondensed chromosomes, irregular microtubule spindles and metaphase plates as well as congression defects) (Figure 5D-G) and higher percentage of aberrant mitoses in comparison to cells from MOmis-injected control embryos (44% versus ~11%, respectively). Similarly, a strong reduction of cells in prophase (~1% versus 25%) and a diminution of cells in anaphase/telophase (~25% versus 35%, Figure 5H) were observed in MOex5 morphants in comparison to control embryos. These results are in agreement with previous observation in human cells in culture showing that MAP9 inhibition led to abnormal spindles and nuclei as well as chromosome congression and segregation defects⁹, and indicate that Map9 is critical for mitosis regulation during zebrafish embryo development.

***Map9* is required for YSL function, epiboly and gastrulation**

Based on the findings that *map9* morphants display gastrulation/epiboly defects (Figure 2) and that mammalian MAP9 binds to MTs and is essential for the correct formation of bipolar mitotic spindles and mitosis completion⁹, we asked whether *map9* could be involved in YSL dynamics³⁰. Indeed, just before the midblastula transition, the zebrafish MT network is necessary for the fusion of the marginal blastomeres with the yolk to form the YSL that will then drive epiboly and gastrulation^{31,32}. During epiboly, YSL nuclei, followed by the blastoderm, spread toward the vegetal pole^{31,33} guided by a MT array oriented along the animal-vegetal axis (Figure 6A)^{7,31,32}.

First, we examined the MT cytoskeleton in MOex5 morphants and MOmis-injected controls at ~4.3 hpf (~30% epiboly) by using an antibody against α -tubulin (red; Figure 6B, C) and confocal

microscopy. At this stage, control embryos displayed dense MT spindles/arrays that expanded towards the vegetal pole (Figure 6B). In MOex5 morphants, MT spindles were often absent in YSL and the yolk MT array was not formed properly. These defects are reminiscent of the phenotype (defective yolk cell MTs) of zebrafish embryos in which *eomesa*, a T-box transcription factor involved in dorsal-ventral patterning, epiboly and endoderm specification, is mutated³⁴. Second, we showed that Map9 is associated to the MT network of the YSL (Figure 6D) as well as to the MTs of the mitotic spindles of YSL nuclei (Figure 6E). Map9 localization on the MT network of the YSL and co-localization with α -tubulin suggest that these MT defects in the YSL are Map9-specific.

Then, we directly injected MOex5 or MOmis (control) together with dextran-rhodamine in the YSL³⁵ at the beginning of its formation ($\sim 2_{3/4}$ -3 hpf, 512-1k cell stage³⁰) and followed the injected embryos up to the end of gastrulation (~ 9 hpf, 80% epiboly). Control embryos developed normally up to 96 hpf, whereas the few MOex5-injected embryos that survived up to 10 hpf ($\sim 20\%$) were abnormal and died before 24 hpf (not shown). MOex5 morphants apparently developed normally up to 30% epiboly (~ 4.7 hpf), without obvious differences with controls (Figure 7A-F), but could not reach 80% epiboly (Figure 7G-L). At this stage, epiboly was stopped, the blastoderm tended to separate from the yolk and embryos died. This phenotype was mostly caused by defects of the YSL MT network that, as a consequence, could not drive epiboly (*i.e.*, the extension of the blastoderm towards the vegetal pole). Previous studies reported similar phenotypes resulting from the premature constriction of the actin-myosin ring of the YSL³⁶. We tried to rescue this phenotype by co-injecting either *map9*-YFP or *map9* mRNA in the YSL, but these experiments were unsuccessful (not shown). Injection of MOex5 in the yolk instead of the YSL did not have any effect (not shown). To ascertain that the observed effects are YSL-specific, we also injected MOex5 or MOmis together with a fluorescent dye in random groups of cells in 64-cell stage embryos (Figure S4). Differently from what observed following injection in 1-cell stage embryos in which all daughter-cells are affected, injection of MOex5 in 64-cell stage embryos did not impair epiboly, gastrulation and normal embryo development. However, while cells in which only the dye was injected contributed to the 24 hpf embryo, cells in which MOex5 and the dye were injected did not. This indicates that *map9* knocking down in individual cells of 64-cell stage embryos only leads to the death of the injected cells. This is

an excellent illustration of the vertebrate developmental plasticity and proves that in the embryo, *map9* activity is mainly cell-autonomous.

Altogether these findings suggest that *map9* is required for two of the main processes of zebrafish development, *i.e.* for individual cell divisions and for YSL to drive epiboly and gastrulation. These processes rely heavily on the YSL MT network.

***Map9* knockdown perturbs different signalling pathways**

Finally, to gain insight into the effects of *map9* knockdown on gene expression, we measured by qRT-PCR, at mid-epiboly, the relative expression of a number of genes involved in the main pathways of early zebrafish development, knowing that changes in gene expression might be indirect effects of *map9* inhibition by perturbing multiple regulation pathways.

RNA was prepared from MOex5 and MOmis (controls) morphants at 7 hpf (50% epiboly, *i.e.* before the onset of embryo death at 9-10 hpf). As already described in Figure 2, *map9* expression (Figure 8) was strongly reduced (x 0.12) in morphants, as a result of a transcriptional block and/or low stability of the mis-spliced zygotic mRNA, or of a feedback loop regulation. First, we examined the expression of genes that are involved in endoderm development³⁷. *Oep* and *eomesa* were overexpressed (x 1.7 and x 3.9 respectively); *eomesb*, *mezzo* (*og9x*) and *sox32* (or *casanova*, *cas*) were down-regulated (x 0.6, 0.5, <0.2 respectively), whereas *gata 5* (*faust*) and *foxa2* displayed variations comprised between 20 and 30%. *Sqt* (or *ndr1* for nodal-related 1), *cyc* (or *ndr2* for nodal-related 2), *tarama* (*acvr1b* or *alk4*), *ntla*, *bon* (or *mixer*) and *sox17* did not show any variation in comparison to control embryos (Figure 8). Surprisingly, the expression of *sox17* and *foxa2* were not or only slightly affected, despite the fact that *sox32* is a direct transcriptional activator of these two genes³⁸. It is therefore possible that the residual *sox32* activity is sufficient to activate *sox17* and *foxa2*, or that at this stage *sox17* and *foxa2* expression is not *sox32*-dependent.

The expression of the mesendodermal marker and organizer-specific gene *gsc*^{39,40} was not affected. We also examined the expression of genes involved in LR patterning, which relies mainly on the function of the KV⁴¹. Although the KV is formed later during segmentation (~11_{2/3} hpf), the expression of *dnah9* (or *lrd1* for left-right dynein-related1), which is responsible for the motility of

monocilia in the KV and the inhibition of which hampers LR specification⁴¹, was moderately down-regulated (25-30%). Conversely, *spaw* (or *ndr3* for nodal-related 3), which is induced by the KV and is restricted to the LPM⁴², was up-regulated (~x9). *Lefty2*, another nodal-induced gene, which is downstream of *spaw* and is expressed in the left LPM of the heart region, was stable as well as *lefty1*, another gene involved in LR patterning. *Charon* (Cerberus-related protein), which inhibits the expression of *spaw* in the right LPM⁴³, was down-regulated (25-30%) in MOex5 morphants in comparison to control MOmis-injected embryos (Figure 8). As Muto *et al.*⁴⁴ recently described mitosis progression defects in *nipbl*-deficient (by MO) zebrafish embryos, we also checked the expression of *nipbla* and *b* and found that they were not affected by *map9* knockdown.

We then measured the expression of a few genes involved in MT dynamics during mitosis and ciliogenesis. *Shha* and *smo* were down-regulated (x 0.3), *plk1* and *plk4* were up-regulated (x 1.4 and x 1.6 respectively), whereas *igu* showed a moderate decrease of about 30% (Figure 8). As a supplementary control, the measure of the expression of 7 representative genes in MOmis-injected embryos revealed no significant variation with respect to non-injected embryos (Figure 8).

In addition, since all gene expression levels were normalized to β -actin, we verified that the relative decrease of gene expression such as *sox32* or *smo* was not the result of a lack of degradation of maternal β -actin transcripts in morphants. Comparison of the qPCR curves (Cp) between morphants and controls indicated that β -actin expression did not change between morphants and controls (not shown). Also, we checked that the apparent increase of gene expression was not due to the repression of miR-430 expression in morphants. Indeed, miR-430 is expressed at the onset of zygotic transcription and promotes clearance of maternal mRNAs. Thus, in mutants defective for miR-430, the mRNAs that are miR-430 targets are not degraded and appear overexpressed with respect to controls⁴⁵⁻⁴⁷. By screening the Targetscan database (http://www.targetscan.org/fish_62/) we found that only *plk4* and *sqt* are potential miR-430 targets. However, we show here that only *plk4* displays a significant increase in morphants (~x 1.62). On the other hand, *spaw* (x 8.8), *eomesa* (x 3.9) and *aurka* (x 2.2) are not miR-430 targets, even considering weak sites (Targetscan). Furthermore, rescue experiments of mutants defective for miR-430 show that the expression of these genes is not modified, indicating that they are most likely not regulated by the expression of other miR-430-

dependent genes (GEO profiles, GDS1771 from Giraldez lab, <http://www.ncbi.nlm.nih.gov/geoprofiles/?term=GDS1771>). To confirm these data, we measured the expression of *tuba8l*, a maternal gene strongly regulated by miR-430⁴⁷. Indeed in mutants defective for miR-430, *tuba8l* appears overexpressed by ~700%⁴⁷. Our results indicate that *tuba8l* expression does not change significantly between controls and 7 hpf morphants (it is even slightly lower by ~13% in morphants) suggesting that miR-430 is not repressed in *map9* morphants (inset, Figure 8).

We then assessed by *in situ* hybridization the expression of *oep*, *sox32* and *sox17*, the function of which is essential for endoderm development. *Oep*, one of the first genes of the nodal cascade, was expressed early in the blastoderm and localized to the dorsal neural plate at 50% epiboly (shield stage, 6 hpf), as previously described⁴⁸, without obvious difference between MOex5 morphants and control embryos (Figure 9). *Sox32* and *sox17* were strongly expressed in the marginal cells of the blastoderm, the YSL and the presumptive endodermal cells from the earliest assessed stage (dome, 4_{1/3} hpf) to the shield (6 hpf) stage in control embryos, as previously described³⁸. Conversely, in MOex5 morphants, their expression was restricted to only a portion of the marginal cells of the blastoderm (Figure 9B8 and C8).

Discussion

In this study we investigated the role of Map9 during zebrafish embryo development. A schematic representation (Figure 10) of the pathways that are deregulated following morpholino-mediated *map9* knockdown in zebrafish embryos recapitulates our findings and helps understanding how its inhibition can lead to profound developmental defects and/or embryo death.

Specifically, Map9 localizes to the mitotic spindle in embryonic cells and morpholino-mediated knockdown of *map9* leads to mitotic defects similar to those observed following inhibition of the mitotic kinase *plk1*¹⁷, that, as also shown in mammalian cells (Eot-Houlier *et al.*¹¹ and references therein), is essential for cell division in eukaryotes⁴⁹. We also showed that MAP9 is phosphorylated by PLK1¹¹ and that it is localized to the spindle pole by PLK1, thus contributing to spindle pole stability. Altogether, these observations suggest that deregulation of the Plk1-Map9 pathway in zebrafish embryos is associated with mitotic defects that can lead to apoptosis, developmental

abnormalities and eventually cell death. Interestingly, other studies in zebrafish linked apoptosis, YSL, cytoskeleton and epiboly^{36,50}.

We also show that morpholino-mediated knockdown of *map9* not only affects the blastula cells, but also the extra-embryonic YSL. Injection of anti-*map9* MOs in 1-cell stage embryos disrupts the MT network of YSL and anti-*map9* MO injection directly in the nascent YSL at a later developmental stage (~3 hpf) prevents normal epiboly progression, while Map9 deficiency in blastula cells leads to cell-autonomous death. Every YSL nucleus is surrounded by a MT array that directs its migration towards the vegetal pole. Interfering with the MT network by exposure to U.V. light or treatment with nocodazole or taxol (a MT stabilizing drug) leads to defective epiboly movements of both the YSL and the blastoderm³¹. In *map9* morphants, the yolk cell longitudinal MT array is defective with large areas without MT and epiboly is hampered, as previously described in *eomesa* mutants³⁴. The deregulated expression of the *eomes* genes in *map9* morphants (overexpression of *eomesa* and down-regulation of *eomesb*) could contribute to the observed phenotype. Similarly, the endodermal marker *sox32*, a fish-specific HMG-box transcription factor, is down-regulated and its expression restricted to only a portion of the marginal cells of the blastoderm in *map9* morphants, as previously reported in the in *eomesa* mutants, as a result of YSL defects³⁴. The restriction of *sox32* and *sox17* expression in endodermal cells could also contribute to the lethal phenotype of *map9* morphants. Moreover, knockdown experiments have shown that Sox17 is necessary for the formation of the Kupffer's vesicle and LR patterning in zebrafish⁵¹.

In addition, *map9* knockdown might affect also the nodal signalling pathways that are induced in the YSL at the onset of gastrulation⁶ to specify the fates of mesodermal and endodermal progenitor cells along the animal-vegetal axis and to establish the LR body axis^{52,53}. In zebrafish, *sqt*, *cyc* and *oep* are part of the YSL nodal signalling pathways⁵⁴. *Sqt* and *cyc* are essential for organizer development and, consequently, also for mesoderm and endoderm formation, whereas *southpaw* (*spaw*), another nodal-related gene, is needed for LR patterning^{40,54}. Since *sqt*, *cyc* and *gsc* are apparently not deregulated in 7-8 hpf *map9* morphants (~75% epiboly), it suggests that *map9* may also have a role in organizer development. Moreover, in *map9* morphants, *spaw* is strongly overexpressed already at 7 hpf, although *spaw* asymmetric expression is required for the establishment of LR asymmetry only

during/after gastrulation⁴⁰. This suggests that early deregulation of this pathway might lead to altered LR patterning. Multiple signalling pathways are involved earlier in dorsal forerunner cells (DFC) specification, and perturbation of DFC maturation and organization leads to failure in KV organogenesis and function at later stages⁵⁵. The propagation of the *spaw* signal⁴² depends on the function of the KV cilia and on the hedgehog signalling pathway^{56, 57}. In this pathway, the sonic hedgehog ligand binds to and activates the patched receptor that triggers the translocation of the G protein-coupled receptor smo to the tip of the cilia, where it allows accumulation of the transcription factor Gli2⁵⁷⁻⁵⁹. The strong down-regulation of *shha*, which is essential for embryo development^{56, 60}, and of *smo* in *map9* morphants together with the overexpression of *plk1* and *plk4*, which play important functions in ciliogenesis⁶¹⁻⁶³, suggest that *map9* depletion may have consequences on the function of the primary cilia and on cilia-dependent signalling pathways as well.

Finally, *map9* inhibition induced the deregulation of many genes involved early in endoderm development and LR patterning. However it is also possible that these deregulations are secondary effects of Map9 inhibition and/or epiboly arrest. Similar observations have been made in *nipbl*-deficient zebrafish⁴⁴ and in *Nipbl*^{+/-} mouse⁶⁴ models of Cornelia de Lange syndrome, in which many genes are mis-expressed following *nipbl* inhibition.

Although the main phenotype of *map9* morphants (*i.e.* gastrulation defects followed by early embryo death) is likely to result from MT-related defects (mitosis defects and YSL-based epiboly failure), it will be important to determine whether the observed gene deregulations are secondary effects and how they contribute to this phenotype.

Acknowledgements

The authors are grateful to Drs. A. Lander, A. Muto, A. Bruce, M. Halpern, T. Lepage and M. Poulain for providing the *sox17*, *sox32*, *oep*, *cyc*, and *sqt* cDNA clones, to C. Gonzalez, Drs M. N'Guyen and K. Kissa for advices and help in manipulating zebrafish embryos, to Dr. Chris Jopling for help in *map9* ISH experiments, and to Dr. A. Renucci for helpful discussions. We also would like to thank Montpellier Rio Imaging facility for microscopy support. We thank Drs. E. Andermarcher and R. Kiernan for the careful reading of the manuscript and the English language corrections. This work

was supported by the CNRS and grants from Association de la Recherche contre le Cancer (ARC N°4027), Ligue Nationale contre le Cancer (Comité Languedoc-Roussillon 2009), and the European Community's Seventh Framework Programme [FP7-PEOPLE-2011-ITN] under grant agreement no. PITN-GA-2011-289209 for the Marie-Curie Initial Training Network FishForPharma. LF was a recipient of a MERT fellowship.

Materials and methods

Zebrafish

Experiments were done using the zebrafish *golden* mutant⁶⁵ purchased through a local company (Antinea) and maintained according to standard protocols⁶⁶. Embryos were obtained by natural spawning of breeding pairs and grown at 28.5°C in tank water. They were injected and staged according to standard procedures. Ages were expressed as hours post-fertilization (hpf).

Ethics statement

All experimental animal procedures were carried out according to the guidelines of the French Council on Animal Care (Arrêté du 27 Décembre 1994, ref RESR9401964A, Annexe I). Experiments were approved by the Ethics Committee for animal experimentation of the authors' institution (Direction départementale de la protection des populations – Hérault).

Cloning and sequencing zebrafish *map9*

The full-length zebrafish *map9* ORF (clone IMAGp998O0412053Q) was ordered from ImaGenes GmbH (Berlin, Germany), sequenced and the sequence deposited in the GenBank database under the accession number JQ768417. A fragment with the same sequence was amplified by RT-PCR using RNA from the *golden* zebrafish line used in the laboratory. The *map9* ORF and a *map9*ΔCter cDNA (lacking the MAP domain corresponding to amino-acids 451-678) were cloned in phase with YFP in the pCS2+ vector. mRNA was *in vitro* transcribed using the mMessage mMachin Kit (Ambion, Life Technologies Corporation).

Injection of morpholino oligomers (MOs)

Translation-blocking *map9* MO (MO-ATG: 5'-CGTCCATCGTAGCTCCCAAAGAAAC-3') and splice-blocking *map9* MO targeting the exon 5 acceptor splice junction (MOex5: 5'-ACAACCTGTTTACATAAAAAGGTGT-3') as well as a control MO similar to MOex5 but with 5 mismatches (Momis, 5'-ACAACGTCTTTAGATAAATACGTGT-3') and the *tp53* MO (5'-TTGATTTTGCCGACCTCCTCTCCAC-3') were purchased from GeneTools (Philomath, OR, USA). MO solutions (1 nL) were injected, with or without 1 ng of dextran-rhodamine, in the cytoplasm of 1-cell stage or 64-cell stage embryos or directly in the YSL. For overexpression assays, *map9*-YFP RNA was injected at the indicated concentrations in 1-cell stage embryos. For the localization of *map9* on the mitotic spindles, 700 pg of *map9*-YFP RNA were injected in 1-cell stage embryos and *map9* was detected using a rabbit anti-GFP antibody (Biovalley, 1:1000) at 24 hpf. For rescue experiments, 1-cell stage embryos were injected with 1pmol MOex5 or 200 pg *map*-YFP RNA, or both.

Apoptosis assay

For TUNEL assays, embryos were fixed in 4% paraformaldehyde overnight, dechorionated, washed in PBS/0.1% Triton X100 (PBT), incubated in equilibration buffer and treated with Terminal Deoxynucleotidyl Transferase in the presence of fluorescein-12-dUTP (DeadEnd Fluorometric TUNEL System, Promega). Embryos were washed in 2X SSC and PBT and incubated with Hoechst 33258 (1/1000 in PBS).

Whole mount immunofluorescence

Embryos at the indicated stages were fixed in 4% paraformaldehyde overnight, washed in 0.1% PBT and permeabilized in 1% PBT at room temperature (RT) for 1h30. After washing in H₂O and PBT, they were incubated in blocking buffer (1% BSA, 1% DMSO, 2% goat serum in PBS) at RT for 30 min and then with primary antibodies overnight at 4°C. Secondary antibodies were added together with Hoechst 33258 (Sigma). Embryos were washed and mounted in FluorSave or PBS/50% glycerol.

The following primary antibodies were used for immunofluorescence: rabbit anti-phosphoSer10-histone H3 (Upstate, 1:200); mouse anti- α -tubulin (Sigma, 1:1000) and mouse anti- γ -tubulin (Abcam, 1:1000). Alexa 488 rabbit and Alexa 555 mouse fluor-conjugated secondary antibodies (Invitrogen) were diluted at 1:1000.

Whole mount in situ hybridization (ISH)

Embryos at the indicated stages were fixed in 4% paraformaldehyde overnight, dechorionated and dehydrated in PBT/methanol. After rehydration, ISH was performed in hybridization buffer (50% formamide, 5X SSC, 0.5mg/ml tRNA, 0.05mg/ml heparin, 10% Tween) using digoxigenin (DIG)-labelled antisense RNA probes synthesized with the DIG RNA Labeling Mix (Roche). Hybridized probes were detected by using alkaline phosphate-conjugated anti-DIG antibodies and visualized with NBT/BCIP (Roche).

The *map9* and *sox17* (cloned in the pCS2+ vector)^{67, 68} antisense RNA probes were synthesized using T7 RNA polymerase (Promega); the *oep* (pCRII-TOPO) and *sox32* (pGEM-T-Easy) probes using Sp6 RNA polymerase (Promega).

Microscopy observation

Embryos were observed using a Leica DM 2500 confocal microscope and the Leica Applications System, an Axiovert 200M Zeiss microscope and the AxioVision Imaging System, or an MVX10 Olympus microscope.

RT-PCR, qPCR

Total RNA from whole zebrafish embryos was isolated using the Nucleospin RNA II kit (Macherey-Nagel). First-strand cDNA was generated using the Superscript III reverse transcriptase (Invitrogen) and qPCR reactions were performed in quadruplicate in 96-well plates in a final volume of 10 μ L, using the SYBR Green I Master reaction mix (Roche) on a 480-Light Cycler instrument (Roche). PCR amplifications were performed with an initial 5-min denaturation step at 95°C followed by 42 cycles (95°C for 20 sec; 56-60°C for 15 sec; 72°C for 15 sec). The relative expression levels of each

target gene was normalized to β -actin as control gene⁶⁹. For quantifying the two *map9* mRNA species (wt and misspliced) in MOex5 morphants, primer pairs specific of wt (ZFovF and ZFdelR1) and misspliced (ZF18F and ZFjctR) mRNAs were used. Primer sequences are listed in Table S1.

References

1. Bonner MK, Poole DS, Xu T, Sarkeshik A, Yates JR, 3rd, Skop AR. Mitotic spindle proteomics in Chinese hamster ovary cells. *PLoS ONE* 2011; 6:e20489.
2. Sauer G, Korner R, Hanisch A, Ries A, Nigg EA, Sillje HH. Proteome analysis of the human mitotic spindle. *Mol Cell Proteomics* 2005; 4:35-43.
3. Karsenti E, Vernos I. The mitotic spindle: a self-made machine. *Science* 2001; 294:543-7.
4. Wittmann T, Hyman A, Desai A. The spindle: a dynamic assembly of microtubules and motors. *Nat Cell Biol* 2001; 3:E28-34.
5. Wadsworth P, Lee WL, Murata T, Baskin TI. Variations on theme: spindle assembly in diverse cells. *Protoplasma* 2011; 248:439-46.
6. Carvalho L, Heisenberg CP. The yolk syncytial layer in early zebrafish development. *Trends in cell biology* 2010; 20:586-92.
7. Carvalho L, Stuhmer J, Bois JS, Kalaidzidis Y, Lecaudey V, Heisenberg CP. Control of convergent yolk syncytial layer nuclear movement in zebrafish. *Development* 2009; 136:1305-15.
8. Bonneau B, Popgeorgiev N, Prudent J, Gillet G. Cytoskeleton dynamics in early zebrafish development: A matter of phosphorylation? *Bioarchitecture* 2011; 1:216-20.
9. Saffin JM, Venoux M, Prigent C, Espeut J, Poulat F, Giorgi D, et al. ASAP, a human microtubule-associated protein required for bipolar spindle assembly and cytokinesis. *Proc Natl Acad Sci U S A* 2005; 102:11302-7.
10. Venoux M, Basbous J, Berthenet C, Prigent C, Fernandez A, Lamb NJ, et al. ASAP is a novel substrate of the oncogenic mitotic kinase Aurora-A : phosphorylation on Ser625 is essential to spindle formation and mitosis. *Hum Mol Genet* 2008; 17:215-24.
11. Eot-Houllier G, Venoux M, Vidal-Eychenie S, Hoang MT, Giorgi D, Rouquier S. Plk1 regulates both ASAP localization and its role in spindle pole integrity. *J Biol Chem* 2010; 285:29556-68.
12. Basbous J, Knani D, Bonneaud N, Giorgi D, Brondello JM, Rouquier S. Induction of ASAP (MAP9) contributes to p53 stabilization in response to DNA damage. *Cell Cycle* 2012; 11.
13. Otto EA, Hurd TW, Airik R, Chaki M, Zhou W, Stoetzel C, et al. Candidate exome capture identifies mutation of SDCCAG8 as the cause of a retinal-renal ciliopathy. *Nat Genet* 2010; 42:840-50.
14. Liu Q, Tan G, Levenkova N, Li T, Pugh EN, Jr., Rux JJ, et al. The proteome of the mouse photoreceptor sensory cilium complex. *Molecular & cellular proteomics : MCP* 2007; 6:1299-317.
15. Andersen JS, Wilkinson CJ, Mayor T, Mortensen P, Nigg EA, Mann M. Proteomic characterization of the human centrosome by protein correlation profiling. *Nature* 2003; 426:570-4.
16. Gherman A, Davis EE, Katsanis N. The ciliary proteome database: an integrated community resource for the genetic and functional dissection of cilia. *Nature genetics* 2006; 38:961-2.

17. Jeong K, Jeong JY, Lee HO, Choi E, Lee H. Inhibition of Plk1 induces mitotic infidelity and embryonic growth defects in developing zebrafish embryos. *Dev Biol* 2010; 345:34-48.
18. Amsterdam A, Nissen RM, Sun Z, Swindell EC, Farrington S, Hopkins N. Identification of 315 genes essential for early zebrafish development. *Proceedings of the National Academy of Sciences of the United States of America* 2004; 101:12792-7.
19. Venoux M, Delmouly K, Milhavet O, Vidal-Eychie S, Giorgi D, Rouquier S. Gene organization, evolution and expression of the microtubule-associated protein ASAP (MAP9). *BMC Genomics* 2008; 9:406.
20. Mathavan S, Lee SG, Mak A, Miller LD, Murthy KR, Govindarajan KR, et al. Transcriptome analysis of zebrafish embryogenesis using microarrays. *PLoS Genet* 2005; 1:260-76.
21. Kimmel CB, Ballard WW, Kimmel SR, Ullmann B, Schilling TF. Stages of embryonic development of the zebrafish. *Dev Dyn* 1995; 203:253-310.
22. Dosch R, Wagner DS, Mintzer KA, Runke G, Wiemelt AP, Mullins MC. Maternal control of vertebrate development before the midblastula transition: mutants from the zebrafish I. *Developmental cell* 2004; 6:771-80.
23. Thisse B, Thisse C. Fast Release Clones: A High Throughput Expression Analysis. . ZFIN Direct Data Submission (<http://zfin.org>) 2004.
24. Adams M, Simms RJ, Abdelhamed Z, Dawe HR, Szymanska K, Logan CV, et al. A meckelin-filamin A interaction mediates ciliogenesis. *Human molecular genetics* 2011.
25. Aspatwar A, Tolvanen ME, Jokitalo E, Parikka M, Ortutay C, Harjula SK, et al. Abnormal cerebellar development and ataxia in CARP VIII morphant zebrafish. *Human molecular genetics* 2013; 22:417-32.
26. Cole LK, Ross LS. Apoptosis in the developing zebrafish embryo. *Developmental biology* 2001; 240:123-42.
27. Jeon HY, Lee H. Depletion of Aurora-A in zebrafish causes growth retardation due to mitotic delay and p53-dependent cell death. *Febs J* 2013.
28. Zhong H, Xin S, Zhao Y, Lu J, Li S, Gong J, et al. Genetic approach to evaluate specificity of small molecule drug candidates inhibiting PLK1 using zebrafish. *Mol Biosyst* 2010; 6:1463-8.
29. Giet R, Glover DM. *Drosophila* aurora B kinase is required for histone H3 phosphorylation and condensin recruitment during chromosome condensation and to organize the central spindle during cytokinesis. *The Journal of cell biology* 2001; 152:669-82.
30. Kimmel CB, Law RD. Cell lineage of zebrafish blastomeres. II. Formation of the yolk syncytial layer. *Developmental biology* 1985; 108:86-93.
31. Solnica-Krezel L, Driever W. Microtubule arrays of the zebrafish yolk cell: organization and function during epiboly. *Development* 1994; 120:2443-55.
32. Lepage SE, Bruce AE. Zebrafish epiboly: mechanics and mechanisms. *Int J Dev Biol* 2010; 54:1213-28.
33. Solnica-Krezel L. Gastrulation in zebrafish -- all just about adhesion? *Current opinion in genetics & development* 2006; 16:433-41.
34. Du S, Draper BW, Mione M, Moens CB, Bruce A. Differential regulation of epiboly initiation and progression by zebrafish Eomesodermin A. *Developmental biology* 2012; 362:11-23.
35. Arrington CB, Yost HJ. Extra-embryonic syndecan 2 regulates organ primordia migration and fibrillogenesis throughout the zebrafish embryo. *Development* 2009; 136:3143-52.

36. Popgeorgiev N, Bonneau B, Ferri KF, Prudent J, Thibaut J, Gillet G. The apoptotic regulator Nr2f1 controls cytoskeletal dynamics via the regulation of Ca²⁺ trafficking in the zebrafish blastula. *Developmental cell* 2011; 20:663-76.
37. Tam PP, Kanai-Azuma M, Kanai Y. Early endoderm development in vertebrates: lineage differentiation and morphogenetic function. *Current opinion in genetics & development* 2003; 13:393-400.
38. Kikuchi Y, Agathon A, Alexander J, Thisse C, Waldron S, Yelon D, et al. casanova encodes a novel Sox-related protein necessary and sufficient for early endoderm formation in zebrafish. *Genes & development* 2001; 15:1493-505.
39. Chen S, Kimelman D. The role of the yolk syncytial layer in germ layer patterning in zebrafish. *Development* 2000; 127:4681-9.
40. Long S, Ahmad N, Rebagliati M. The zebrafish nodal-related gene southpaw is required for visceral and diencephalic left-right asymmetry. *Development* 2003; 130:2303-16.
41. Essner JJ, Amack JD, Nyholm MK, Harris EB, Yost HJ. Kupffer's vesicle is a ciliated organ of asymmetry in the zebrafish embryo that initiates left-right development of the brain, heart and gut. *Development* 2005; 132:1247-60.
42. Wang X, Yost HJ. Initiation and propagation of posterior to anterior (PA) waves in zebrafish left-right development. *Developmental dynamics : an official publication of the American Association of Anatomists* 2008; 237:3640-7.
43. Hashimoto H, Rebagliati M, Ahmad N, Muraoka O, Kurokawa T, Hibi M, et al. The Cerberus/Dan-family protein Charon is a negative regulator of Nodal signaling during left-right patterning in zebrafish. *Development* 2004; 131:1741-53.
44. Muto A, Calof AL, Lander AD, Schilling TF. Multifactorial Origins of Heart and Gut Defects in nipbl-Deficient Zebrafish, a Model of Cornelia de Lange Syndrome. *PLoS biology* 2011; 9:e1001181.
45. Bazzini AA, Lee MT, Giraldez AJ. Ribosome profiling shows that miR-430 reduces translation before causing mRNA decay in zebrafish. *Science* 2012; 336:233-7.
46. Giraldez AJ, Cinalli RM, Glasner ME, Enright AJ, Thomson JM, Baskerville S, et al. MicroRNAs regulate brain morphogenesis in zebrafish. *Science* 2005; 308:833-8.
47. Giraldez AJ, Mishima Y, Rihel J, Grocock RJ, Van Dongen S, Inoue K, et al. Zebrafish MiR-430 promotes deadenylation and clearance of maternal mRNAs. *Science* 2006; 312:75-9.
48. Thisse B, Pflumio, S., Fürthauer, M., Loppin, B., Heyer, V., Degraeve, A., Woehl, R., Lux, A., Steffan, T., Charbonnier, X.Q. and Thisse, C. Expression of the zebrafish genome during embryogenesis. ZFIN Direct Data Submission (<http://zfin.org>) 2001.
49. Petronczki M, Lenart P, Peters JM. Polo on the Rise-from Mitotic Entry to Cytokinesis with Plk1. *Developmental cell* 2008; 14:646-59.
50. Arnaud E, Ferri KF, Thibaut J, Haftek-Terreau Z, Aouacheria A, Le Guellec D, et al. The zebrafish bcl-2 homologue Nr2f1 controls development during somitogenesis and gastrulation via apoptosis-dependent and -independent mechanisms. *Cell death and differentiation* 2006; 13:1128-37.
51. Aamar E, Dawid IB. Sox17 and chordin are required for formation of Kupffer's vesicle and left-right asymmetry determination in zebrafish. *Developmental dynamics : an official publication of the American Association of Anatomists* 2010; 239:2980-8.
52. Hagos EG, Dougan ST. Time-dependent patterning of the mesoderm and endoderm by Nodal signals in zebrafish. *BMC Dev Biol* 2007; 7:22.
53. Fan X, Hagos EG, Xu B, Sias C, Kawakami K, Burdine RD, et al. Nodal signals mediate interactions between the extra-embryonic and embryonic tissues in zebrafish. *Developmental biology* 2007; 310:363-78.

54. Feldman B, Gates MA, Egan ES, Dougan ST, Rennebeck G, Sirotkin HI, et al. Zebrafish organizer development and germ-layer formation require nodal-related signals. *Nature* 1998; 395:181-5.
55. Matsui T, Bessho Y. Left-right asymmetry in zebrafish. *Cellular and molecular life sciences : CMLS* 2012; 69:3069-77.
56. Wilson CW, Stainier DY. Vertebrate Hedgehog signaling: cilia rule. *BMC Biol* 2010; 8:102.
57. Goetz SC, Anderson KV. The primary cilium: a signalling centre during vertebrate development. *Nature reviews Genetics* 2010; 11:331-44.
58. May SR, Ashique AM, Karlen M, Wang B, Shen Y, Zarbali K, et al. Loss of the retrograde motor for IFT disrupts localization of Smo to cilia and prevents the expression of both activator and repressor functions of Gli. *Dev Biol* 2005; 287:378-89.
59. Jiang J, Hui CC. Hedgehog signaling in development and cancer. *Developmental cell* 2008; 15:801-12.
60. McMahon AP, Ingham PW, Tabin CJ. Developmental roles and clinical significance of hedgehog signaling. *Curr Top Dev Biol* 2003; 53:1-114.
61. Bettencourt-Dias M, Glover DM. Centrosome biogenesis and function: centrosomes brings new understanding. *Nat Rev Mol Cell Biol* 2007; 8:451-63.
62. Bettencourt-Dias M, Hildebrandt F, Pellman D, Woods G, Godinho SA. Centrosomes and cilia in human disease. *Trends in genetics : TIG* 2011; 27:307-15.
63. Carvalho-Santos Z, Machado P, Branco P, Tavares-Cadete F, Rodrigues-Martins A, Pereira-Leal JB, et al. Stepwise evolution of the centriole-assembly pathway. *J Cell Sci* 2010; 123:1414-26.
64. Kawachi S, Calof AL, Santos R, Lopez-Burks ME, Young CM, Hoang MP, et al. Multiple organ system defects and transcriptional dysregulation in the Nipbl(+/-) mouse, a model of Cornelia de Lange Syndrome. *PLoS Genet* 2009; 5:e1000650.
65. Lamason RL, Mohideen MA, Mest JR, Wong AC, Norton HL, Aros MC, et al. SLC24A5, a putative cation exchanger, affects pigmentation in zebrafish and humans. *Science* 2005; 310:1782-6.
66. Westerfield M. *The Zebrafish Book: A Guide for the Laboratory Use of Zebrafish (Danio rerio)*. Eugene: University of Oregon Press, 2007.
67. Halpern ME, Hatta K, Amacher SL, Talbot WS, Yan YL, Thisse B, et al. Genetic interactions in zebrafish midline development. *Developmental biology* 1997; 187:154-70.
68. Poulain M, Lepage T. Mezzo, a paired-like homeobox protein is an immediate target of Nodal signalling and regulates endoderm specification in zebrafish. *Development* 2002; 129:4901-14.
69. Hellems J, Mortier G, De Paepe A, Speleman F, Vandesompele J. qBase relative quantification framework and software for management and automated analysis of real-time quantitative PCR data. *Genome Biol* 2007; 8:R19.

Figure legends

Figure 1

Expression of *map9* in early zebrafish embryos. (A) Relative quantification of *map9* mRNA by qPCR in 0 hpf (unfertilized eggs) to 24 hpf embryos. Data are the mean \pm SD from three independent experiments, with n=25-35 embryos per time point (**p* <0.005 by Student's *t* test). (B-C) Subcellular

localization of Map9 during mitosis in 24 hpf embryos following expression of *map9*-YFP. 700 pmol of *map9*-YFP RNA was injected at the 1-cell stage, embryos fixed at 24 hpf, and stained with an anti- α -tubulin antibody (red) and Hoechst 33258. Confocal microscopy images show that Map9-YFP (green) co-localizes with α -tubulin on the microtubules of the mitotic spindle (B). In interphase cells (C), Map9-YFP co-localizes with γ -tubulin (red) at centrosomes. (Scale bars, 10 μ m).

Figure 2

MO-mediated depletion of *map9* leads to early defects and/or embryo death and growth failure. (A) Injection of splice-blocking MOex5 leads to the production of a mis-spliced *map9* mRNA. RT-PCR was performed using *map9* specific primers and RNA from embryos injected at the 1-cell stage with MOex5 (5 and 8 hpf), translation-blocking MO-ATG (8 hpf) or the control MOmis (8 hpf). PCR products were separated on 0.8% agarose gels. MOex5 PCR products show two bands that differ by \sim 300 bp in size. (B) Top, subcloning and sequencing of these two fragments revealed that the upper band corresponds to wild-type (wt) *map9*, whereas the lower band corresponds to an mRNA in which exon 5 and 6 are deleted. mRNA from MO-ATG and MOmis-injected embryos show only wt *map9*. The position of MOex5 is indicated by an arrow on the acceptor splice junction of exon 5. Exons 5 and 6 are shaded in grey, and black boxes represent untranslated regions. Bottom, measure by qPCR of the expression of the two *map9* mRNA forms in 8 hpf MOex5 and MO-ATG morphants. In MOex5 morphants the expression of *map9* is \sim 5 times lower than in MO-ATG morphants, and the misspliced forms represents 11% of *map9* mRNA versus background level $<$ 1% in MO-ATG morphants (inset). (C-F) 1-cell stage zebrafish embryos were injected with 1 pmol of anti-*map9* MOex5 or control MOmis and imaged at mid-epiboly. Growth and epiboly in MOex5 morphants are arrested very early. (G-L) Embryos at 24 and 48 hpf after injection of 0.25 pmol of the two MOs. *Map9* morphants show complex malformations, including underdeveloped nervous system, absence of the eyes, abnormal yolk, notochord (I and J, arrow in the insets), somites and tail (J, arrowheads) and pericardial oedema (L, arrowhead). In I and J, the insets are enlargements of the dotted boxes.

Figure 3

Map9-YFP RNA can partially rescue the phenotypes of MOex5 morphants. (A) Embryos were injected at the 1-cell stage with 1 pmol MOex5, 200 pg *map9*-YFP RNA or both. *Map9*-YFP-injected embryos developed normally up to mid-epiboly and later stages. 40% of MOex5 morphants showed defects at mid-epiboly and 20% were blocked at the sphere stage. Following co-injection of MOex5 and *map9*-YFP RNA, about 80% of embryos developed normally up to mid-epiboly, but died at ~9-10 hpf. (B) Representative images of embryos injected with *map9*-YFP RNA (at mid-epiboly, n=102), with MOex5 (showing developmental delay and defects before mid-epiboly, n=85) or with both MOex5 and *map9*-YFP RNA (showing partial rescue of the phenotype at mid-epiboly, n=153). Scale bars, 200 μ m.

Figure 4

Morpholino-mediated depletion of *map9* leads to increased apoptosis. (A-D) Zebrafish embryos were injected, or not (control), at the 1-cell stage with 1 pmol of MOex5 for observation at 8 hpf, or with 0.25 pmol MOex5 for observation at 24 hpf. TUNEL-positive cells (green) were counted in injected (B, D) and control embryos (A, C) (n=10/assay). (E) Left panel, number of TUNEL-positive cells in the control and MOex5-injected embryos depicted in A-D, n= 5 embryos per assay, total cell count ~1070 (* $p < 0.005$, ** $p < 0.02$); right panel, tp53 inhibition does not rescue apoptosis induced by MOex5. Number of TUNEL-positive cells in MOex5- and MOex5 + MOtp53-injected embryos (n=20 embryos per assay, total cell count ~564). (F) Map9 depletion does not induce tp53 expression. Embryos were injected at the 1-cell stage with 1 pmol of MOex5. RNA from 7 hpf *map9* morphants and control embryos was used to quantify *tp53* gene expression by RT-qPCR. Expression data were normalized to β -actin. Experiments were made in quadruplicate, n=42 control embryos and 50 MOex5 morphants at 7 hpf, and n=39/44 embryos at 24 hpf. (G) Co-injection of MOex5 (1 pmol) and MOtp53 (0.5 pmol) does not rescue MOex5 effects. Embryo mortality was not rescued after tp53 depletion by morpholino. Embryo mortality after injection of a control MO (MOmis) was not significantly different compared to non-injected embryos. This experiment was made in duplicate.

Figure 5

Morpholino-mediated depletion of *map9* leads to a reduction in the number of mitotic cells and to mitotic defects. (A, B) Embryos were injected at the 1-cell stage with 1 pmol MOex5 or MOMis (control) and stained with the anti-phosphorylated histone H3 (pH3) antibody (red). DNA was labelled with Hoechst 33258 (blue). Scale bars, 200 μ m. (C) pH3-positive mitotic cells were counted in injected embryos at 5 hpf (n=10/group). In MOex5 morphants the number of mitotic cells was reduced by ~40% in comparison to controls. Similar results were obtained in 8 hpf embryos (not shown). (D-G) Embryos were injected at the 1-cell stage with 1 pmol MOMis (control) (D-E) or MOex5 (F-G) and mitotic cells were imaged in 8 hpf embryos by confocal microscopy (scale bars, 10 μ m). DNA was labelled with Hoechst (green) and MTs of the mitotic spindles with an anti- α -tubulin antibody (red). (H) Percentage of cells at different phases of mitosis. Mitotic cells were scored in *map9* morphants and control embryos (n=10 embryos/assay).

Figure 6

Microtubules in the YSL are disorganized in *map9* morphants. (A) Schematic representation of the organization of the YSL and yolk cell MT array in early zebrafish embryos (adapted from [43]). The portion boxed in blue represents the region analysed in B, C, D. (B, C) Embryos were injected at the 1-cell stage with 1 pmol of control MOMis (B) or MOex5 (C) and imaged by confocal microscopy at ~4.3 hpf (beginning of epiboly). The MT spindles/array are dense and clearly identified in MOMis-injected embryos, whereas they are depleted in MOex5 morphants. (D) Map9 localizes on the MT network of the YSL. *Map9*-YFP, YFP and *map9* RNA (200 pg) were injected separately in 1-cell-stage embryos and imaged at 4.3 hpf. The MT network is labelled with an anti- α -tubulin antibody (red), and Map9-YFP is labelled with an anti-GFP antibody. Nuclei are stained with Hoechst 33258. (E) *Map9*-YFP RNA was injected in 1-cell stage embryos. Map9 colocalizes with α -tubulin on the mitotic spindles of YSL nuclei, (scale bars, 20 μ m).

Figure 7

Inhibition of *map9* expression in the YSL blocks epiboly. (A-L) At the beginning of YSL formation (2_{3/4}-3 hpf), 1 pmol of control MOmis or MOex5 and dextran-rhodamine (red) were co-injected in the YSL. Embryos were observed at 4_{2/3} hpf (30% epiboly) and at ~8 hpf (80% epiboly). Scale bars, 200 μm.

Figure 8

Depletion of *map9* deregulates the expression of genes involved in different signalling pathways. Embryos were injected at the 1-cell stage with 1 pmol of MOex5 or MOmis (controls). RNA from 7 hpf *map9* morphants and control embryos was used to quantify gene expression by RT-qPCR. Expression data were normalized to β-actin. Results are presented as the relative quantification of gene expression in MOex5 morphants and control embryos (C). For each gene, the morphant/control ratio is indicated below the graph, with the lowest and highest values surrounded by a square. Inset, relative quantification of *tuba8l*, a maternal and miR-430 target gene whose expression during the early stages of development relies on miR-430 expression. Experiments were made in quadruplicate, n=42 control embryos and 50 MOex5 morphants.

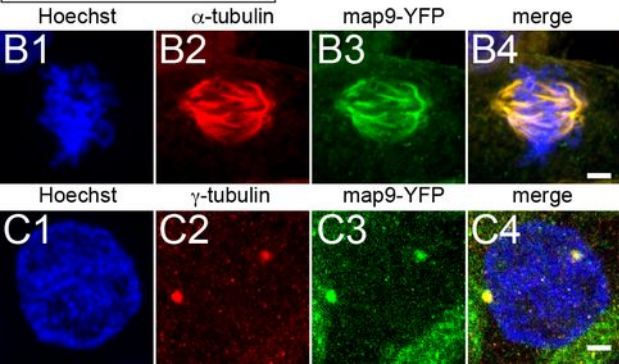
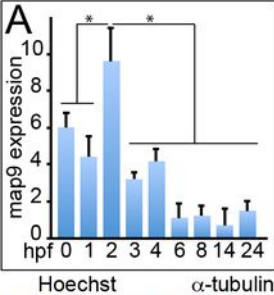
Figure 9

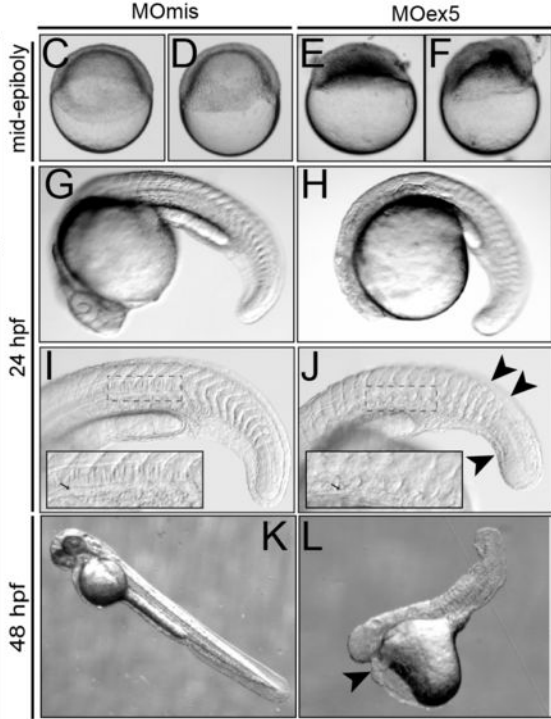
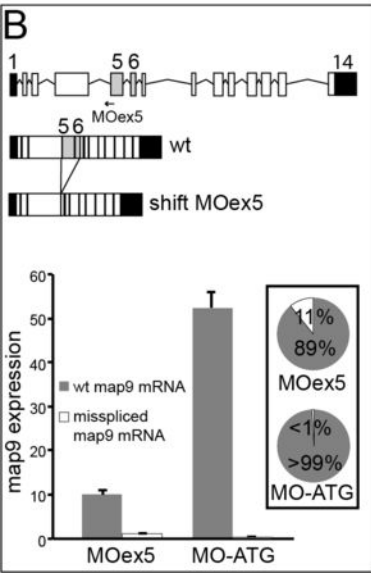
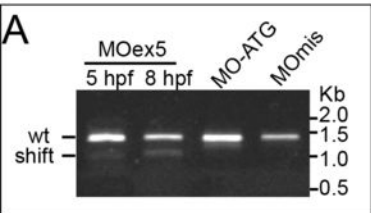
In situ hybridization of selected genes of the nodal pathway that are involved in endoderm development. Embryos injected at the 1-cell stage with 1 pmol of control MOmis or MOex5, were fixed at the indicated times that correspond in MOmis-injected control embryos to the following developmental stages: dome (4_{1/3} hpf), germ-ring (5_{2/3} hpf) and shield (6 hpf). *In situ* hybridization was carried out using antisense *oep* (nodal co-receptor), *sox32* (downstream of *oep*) and *sox17* (activated by *sox32* and required for endoderm specification) RNA probes. In *map9* morphants, expression of *sox32* and *sox17* was restricted to a portion of the blastoderm margin at the shield stage (arrowheads, B8, C8).

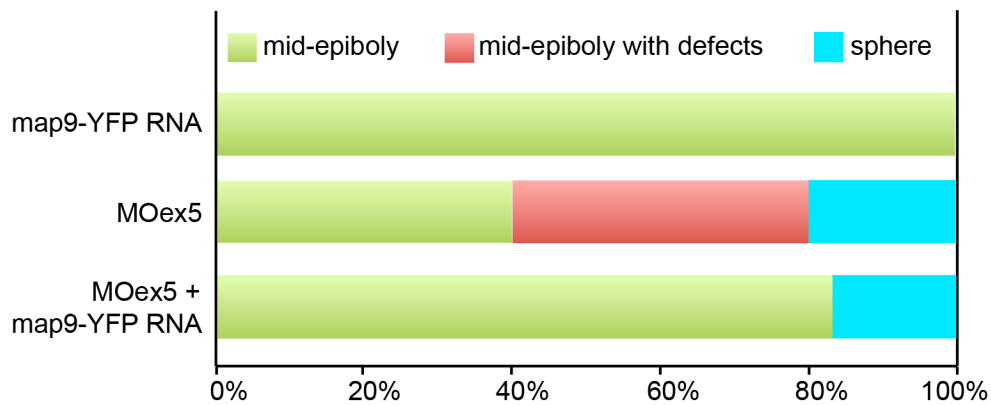
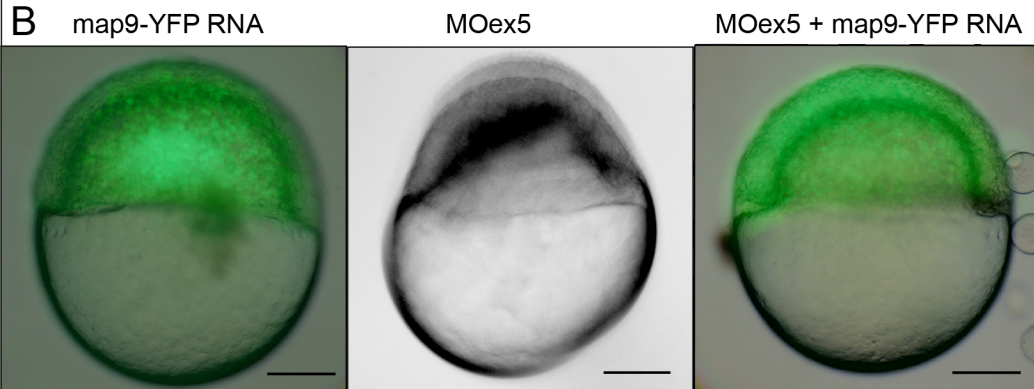
Figure 10

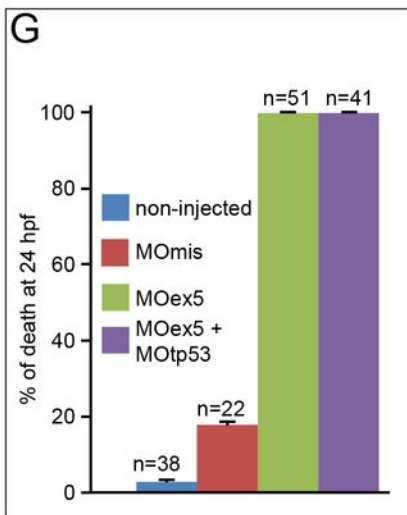
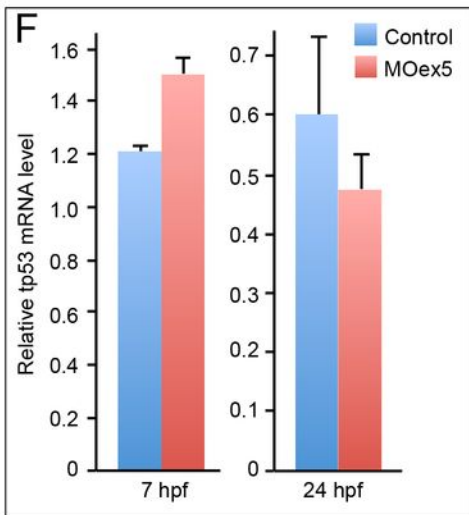
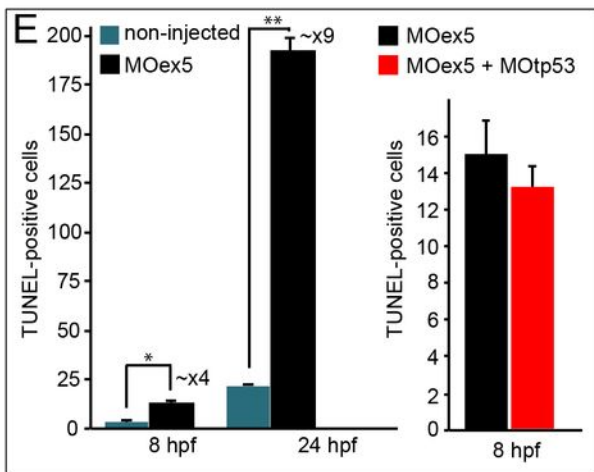
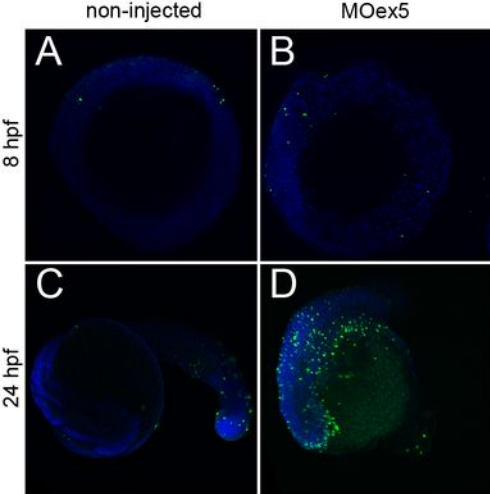
Tentative model for the role of Map9 in zebrafish development. Map9 is required for MT dynamics.

MTs are key components of the mitotic spindle (mitosis) and cilia. MTs and mitosis are essential for the formation of the YSL and epiboly. YSL is required for endoderm development and nodal signalling and the cilia of the KV are responsible for propagating nodal signals involved in left/right asymmetry. As indicated on the schematic, most of these pathways are interdependent. Black arrows indicate the possible role of Map9 during zebrafish development suggested by this and previous studies^{9-11,19}, and grey arrows summarize literature data.

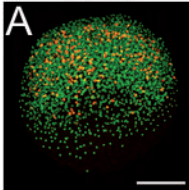




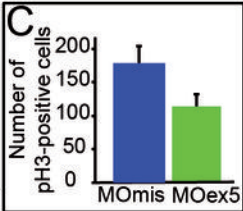
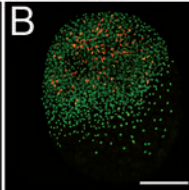
A**B**



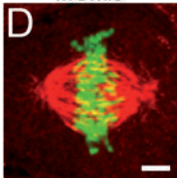
MOmis



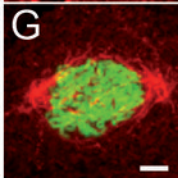
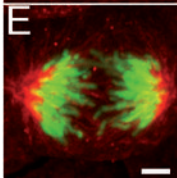
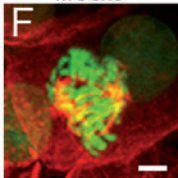
MOex5



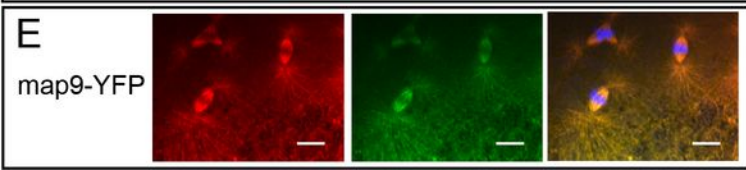
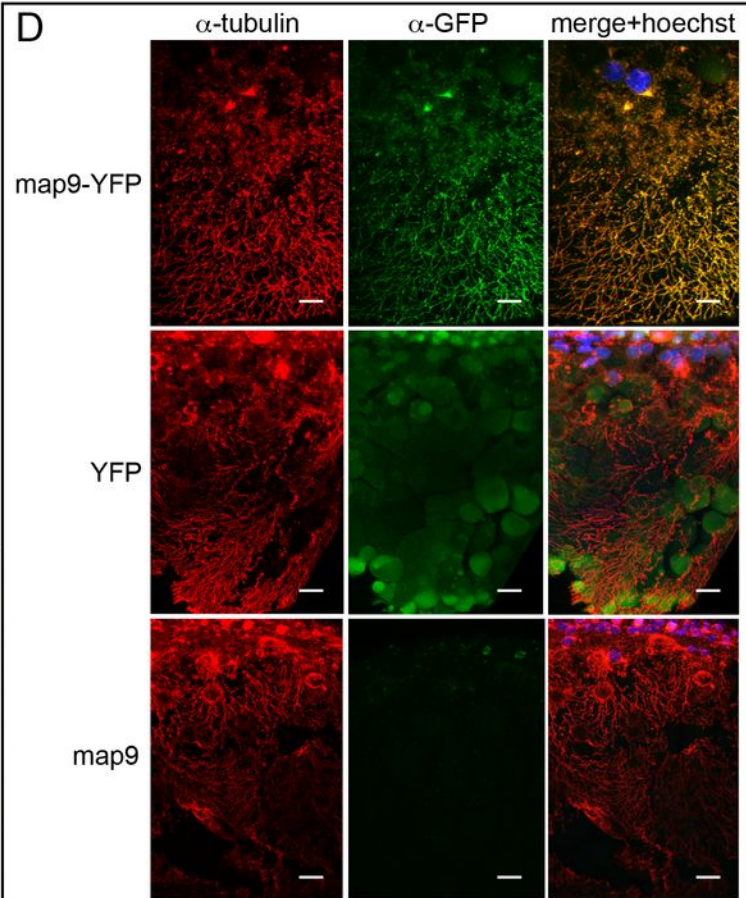
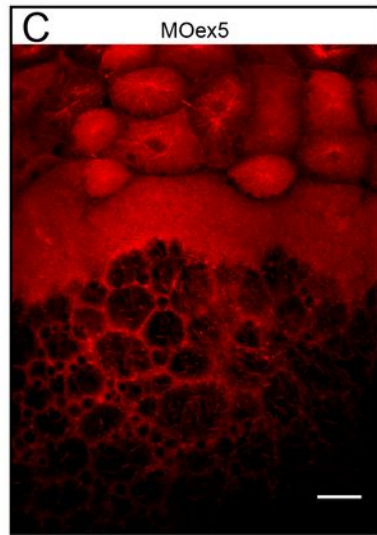
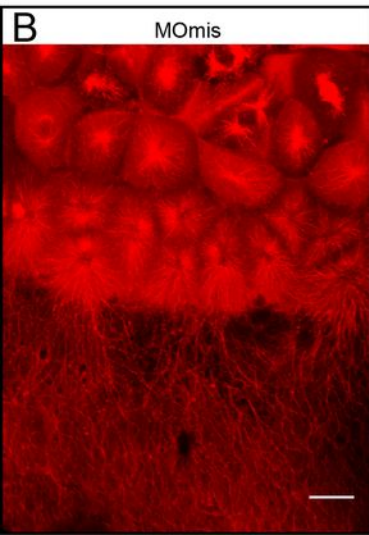
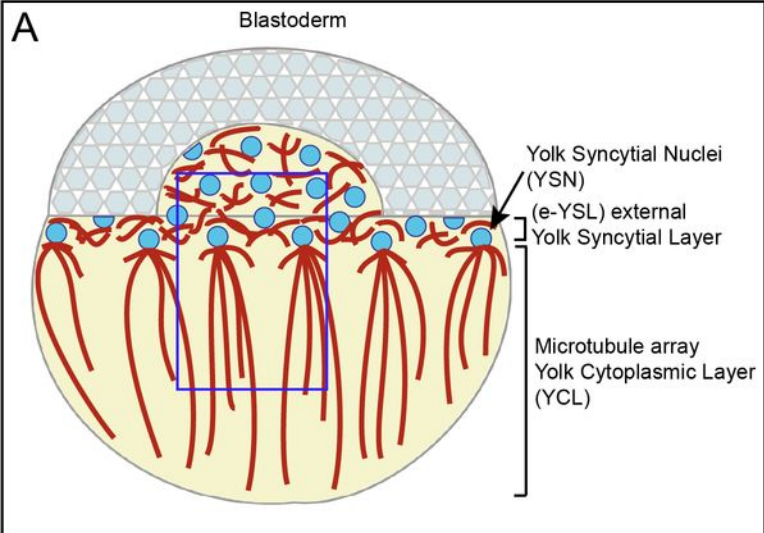
MOmis



MOex5

**H**

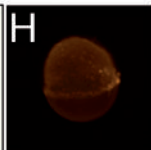
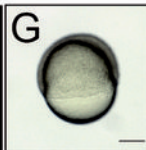
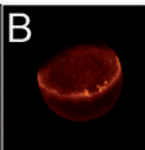
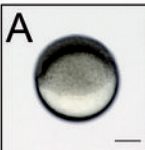
	Momis	Moex5
Prophase	25.4%	0.9%
Metaphase	28.2%	30.0%
Anaphase	35.2%	25.3%
Defects	11.3%	43.7%



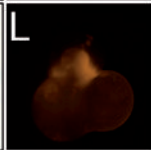
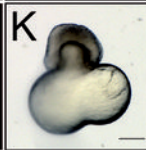
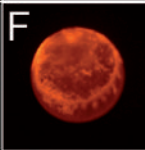
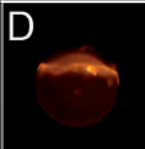
30% epiboly

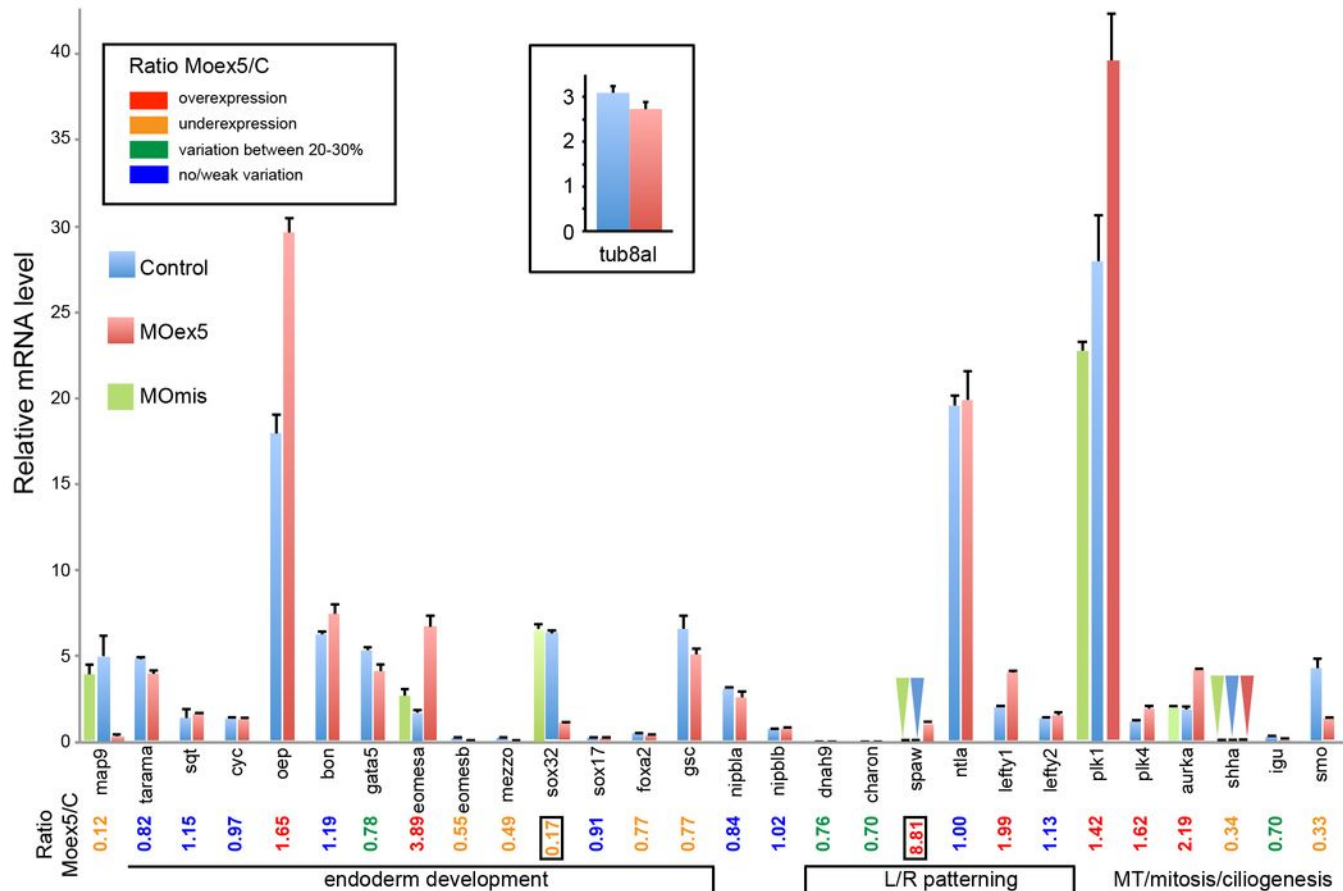
80% epiboly

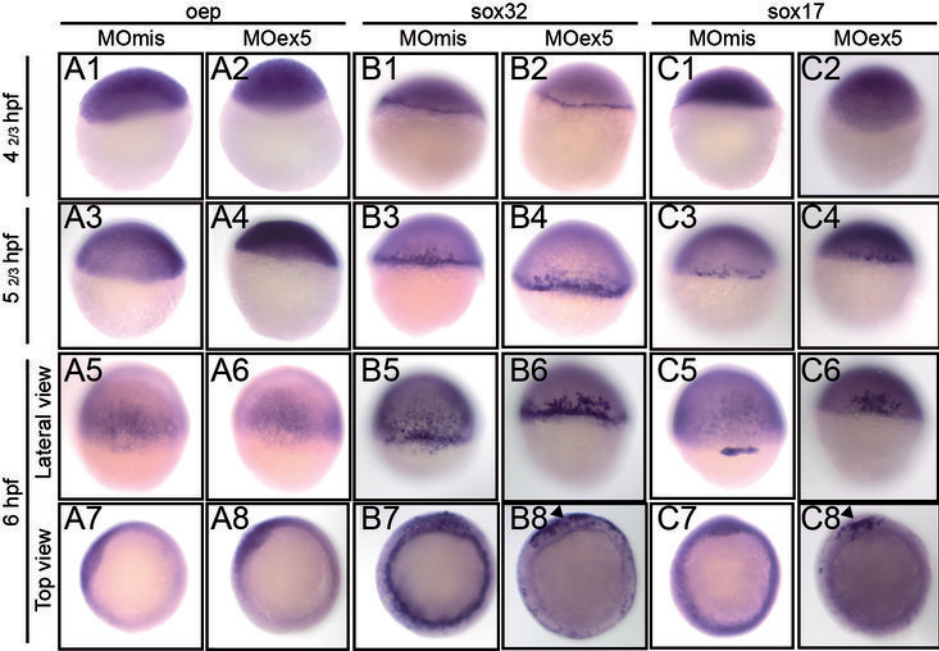
MOmis

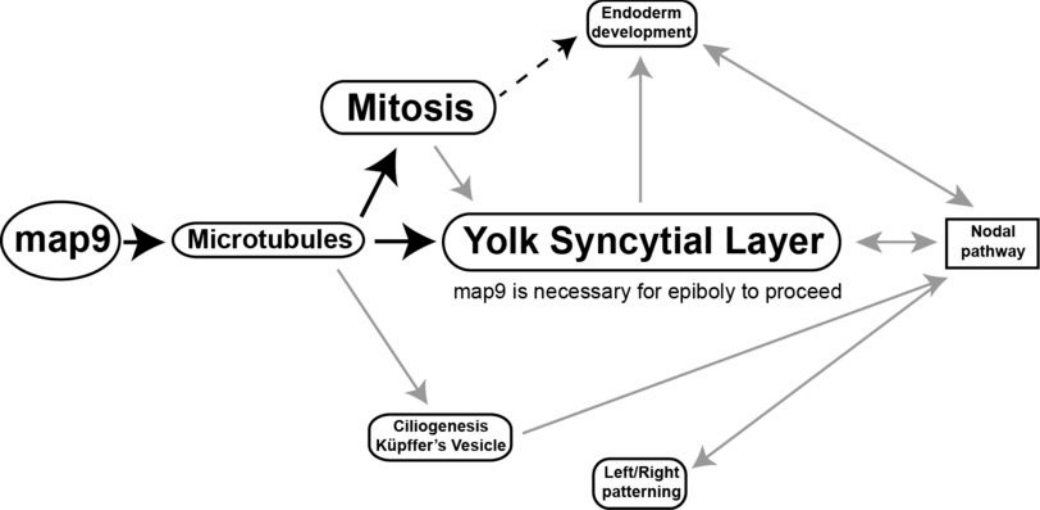


MOex5









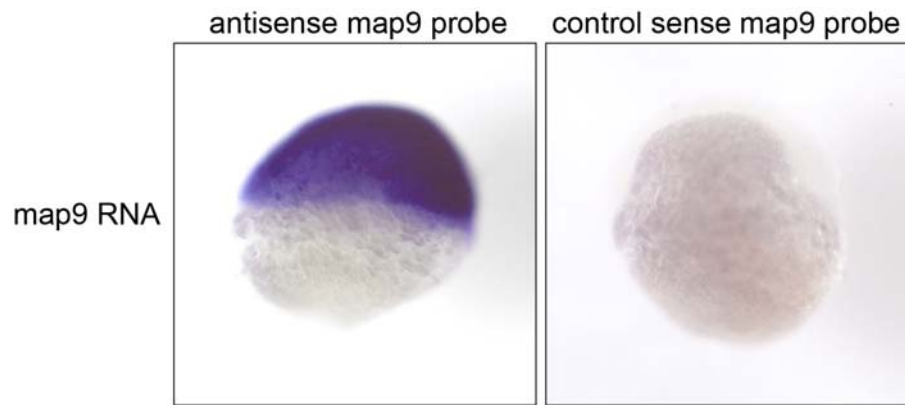


Figure S1

Embryos at the 1-cell stage were injected with 200 pg of *map9* RNA. *In situ* hybridization with either antisense or sense *map9* RNA probes at 30% epiboly (~4.6 hpf) show that *map9* is distributed ubiquitously in the blastoderm.

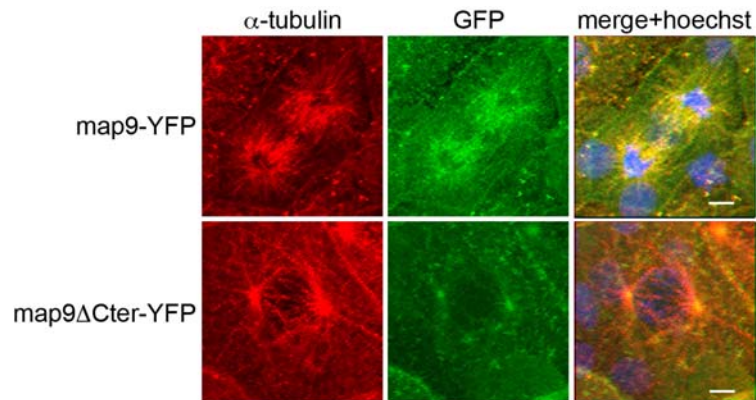


Figure S2

Loss of the fiber-like distribution of Map9 lacking its C-terminal MAP domain in mitotic cells. Map9-YFP or MAP9 Δ Cter-YFP RNA (200 pg) was injected in 1-cell stage embryos. Embryos were fixed at 24 hpf and stained with anti- α -tubulin, anti-GFP antibodies and Hoechst 33258. Confocal microscopy images show that Map9-YFP but not MAP9 Δ Cter-YFP co-localizes with α -tubulin on the microtubules of the mitotic spindle. (Scale bars, 10 μ m).

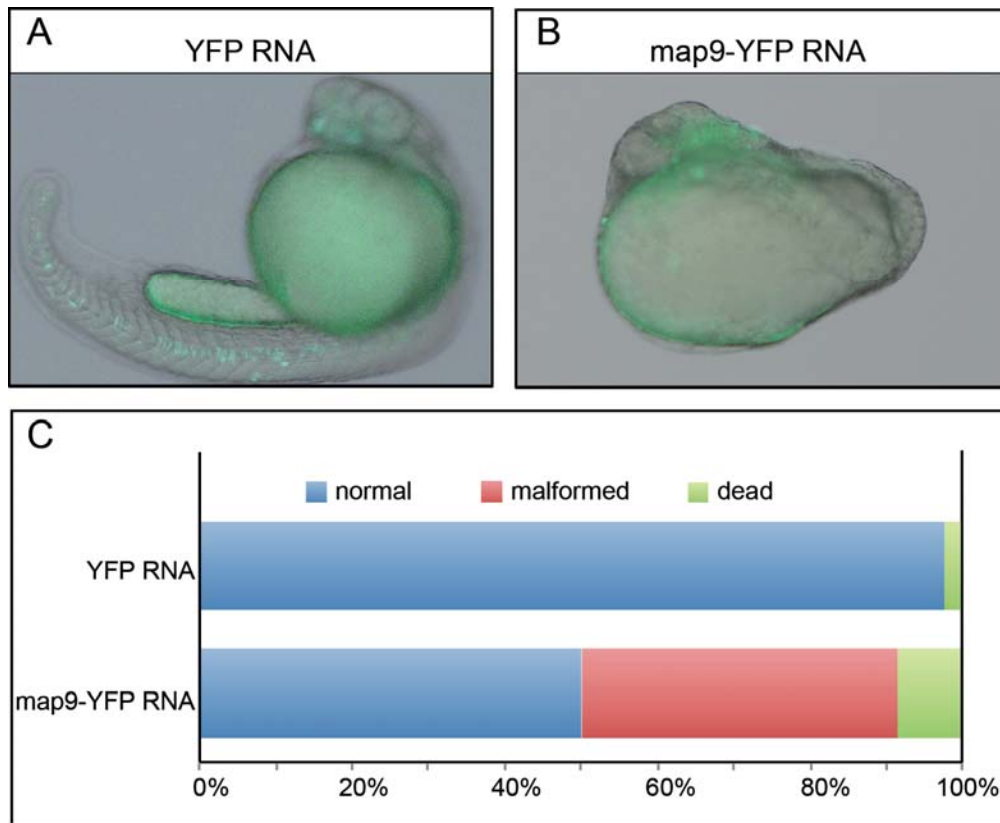


Figure S3

Map9 overexpression is associated with developmental defects and embryo death. (A-B) Embryos were injected with 400 pg YFP RNA, n=42 (A) or *map9*-YFP mRNA, n=36 (B) at the 1-cell stage and imaged at 24 hpf. Scale bars, 200 μ m. (C) Percentages of normal, malformed and dead embryos at 24 hpf.

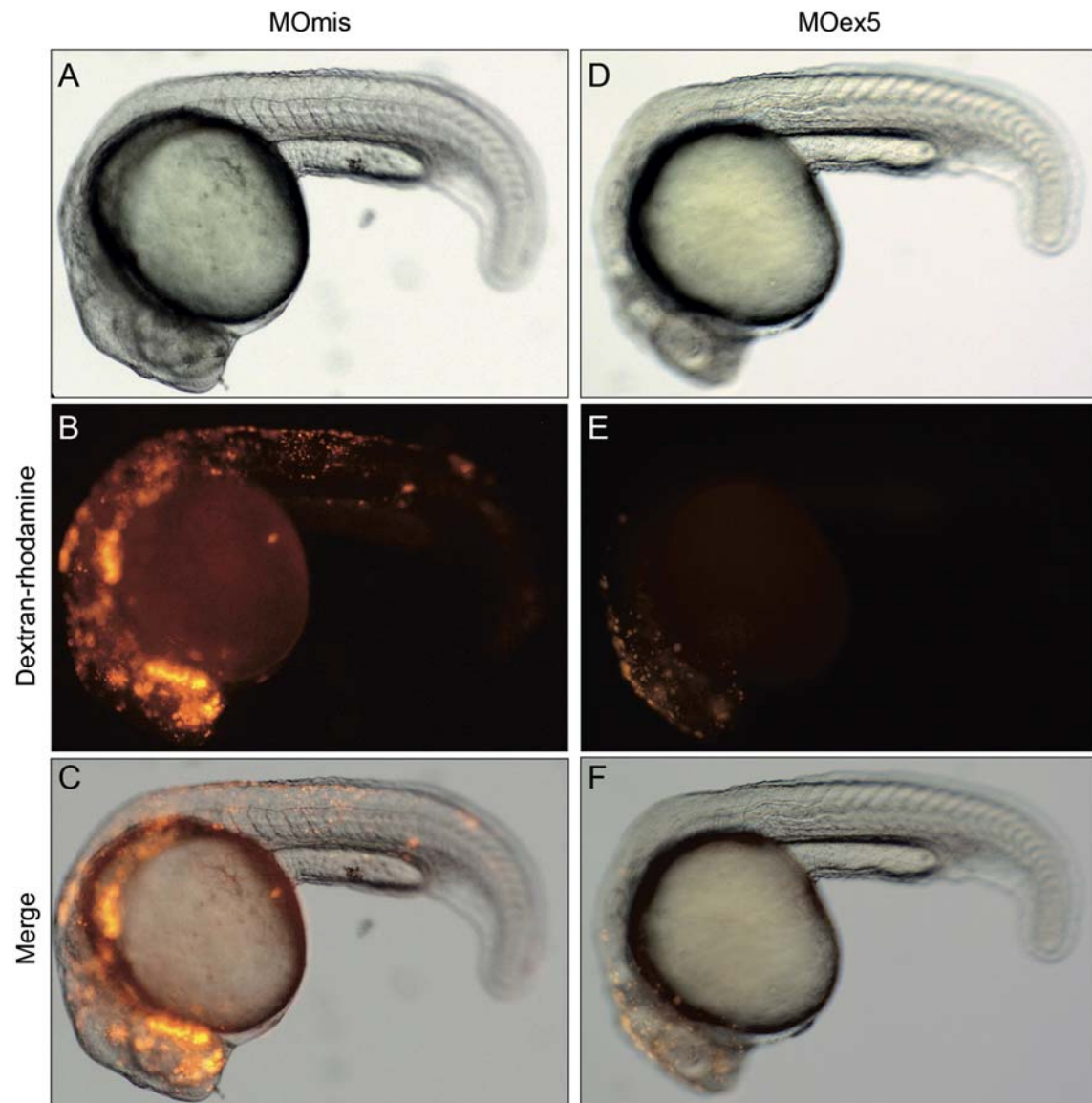


Figure S4

Morpholino-dependent depletion of *map9* in a random group of cells does not affect epiboly. One μg of MOex5 or control MOMis was co-injected with dextran-rhodamine (red) in a group of cells of 64-cell stage embryos. In contrast to embryos injected at the 1-cell stage (Figure 2) or injected directly in the YSL (Figure 6), these embryos do not exhibit developmental defects at 24 hpf.

Primer name	5'-3' sequence
map9 ZF1 fwd	ATGATGACGACGATATACTCA
map9 ZF2 rev	TTAGTGGCAGTGGAGATTC
map9 ZF8 rev	GCCCTCCTAGTAATTTCCAAG
map9 ZF18F	TCCAGTGCCATTGCCTTCAG
map9 ZFjctR	TTCTGTGGCAGCTGCTGACGAT
map9 ZFovF	TCTGTGGCAGCACTGCCAG
map9 ZFdelR1	TCTAACTGGCCAGTGTACAC
aurka fwd	ATTGCAGATTTTGGCTGGTC
aurka rev	TTCTCATCATGTGTTTTACCTTCAA
plk1 fwd	GCCATTCACAAAAGTCTCG
plk1 rev	GCCCTCCTAGTAATTTCCAAG
plk4 fwd	AGGCCTCATTCTCGCTACC
plk4 rev	CTGCTGTGACCGCTCATGTCT
shha fwd	GCAGAAGAAGACATCCGAAGA
shha rev	GGCCAGTGGTTCATTACAGA
smo fwd	AATTGGCCATGTGGTCTG
smo rev	CTTCATTCTGGCAACCCTTAG
igu fwd	TCAATGCGGTGACGTTCTGT
igu rev	AAGGCCTTTTCCACAATGTTGG
gsc fwd	AGAGACGACACCGAACCATTT
gsc rev	GATTCCTCTGACGACGACCTT
oep fwd	TTCGTTGGACTGACCGGAGTT
oep rev	ATCCCTGAGGCGTTCATCGTA
sqt fwd	CCGGACACTTCTGACTGGA
sqt rev	TCGCTTGCTGATATGGAGGAC
cyc fwd	CTGCTCGGAGTGTTCCGAAAG
cyc rev	GTCAAAGATCGCCACGTAG
mezzo fwd	GCTCACGCTGCTTCCAGAGAG
mezzo rev	TGTGGCCAGGGATTCAGAG
ntla fwd	CCTCGGGTTCGTA CTGTGAG
ntla rev	TCCGGAAGAGTTGTCCATGT
sox17 fwd	TCCGCTCTCAGACTCCAAAT
sox17 rev	AATCGCTTGTTTCGTTTCACC
sox32 fwd	ACGAAAGAGGAGCGCAGA
sox32 rev	CATTGCTTTCCATGTCTTGC
tarama fwd	TCAACCTCCAGATTCCCAAT
tarama rev	CTACCGGACCCCAACTACCT
charon fwd	CACAAAAGCGAGCGAAAAA
charon rev	AGCCCTCCTCCGTTATGC
dnah9 fwd	CGCTTCAGGTCTGGAACACT
dnah9 rev	TGAGCCTCGGCTGCTATC
lefty1 fwd	CCAAGTGTGTCCACTTCACAA
lefty1 rev	TCACGGTCTTTGTTGTTTTCA
lefty2 fwd	CCACACAGGATCCAAAGGA
lefty2 rev	GCTGGAGTTACAGTTGCC
spaw fwd	GTCTTGAGCTTGATTGCACA
spaw rev	CGTCTGGATGCAGAAAAC
foxa2 fwd	CAAAATGGAGGGACACGAAC
foxa2 rev	TGTTGCTGACCGAGGTGTAA
nipblA fwd	GAGGCTCCAGTCCCAAGAAT
nipblA rev	CCGGTTCTCCTTGACTTCC
nipblB fwd	GCTGACGGAGCAGTACTACGA
nipblB rev	TGATCACCTCTTCCTCACA
bon fwd	TTTTTCCAAACGCGGATATG

bon rev	TCCTGAAGCGCATAATCTGA
gata5 fwd	GGACGCCAGGGA ACTCTAC
gata5 rev	ACACGGCAGGTCATCCAG
eomesa fwd	CAAAAGGCTTCAGGGACAAT
eomesa rev	AGTAGGAGAGGGCGTCAGTCT
eomesb fwd	CGCGAACATCAACACTTCA
eomesb rev	GTCGTCCGACACCTCCAC

Table S1

Sequences of the primer pairs used to quantify gene expression by qPCR.